Journal of
Mechanical
Science and
Technology

Journal of Mechanical Science and Technology 21 (2007) 465~475

Modeling of Eddy Current Sensor using Geometric and Electromagnetic Data

Tae-Ok Kim[a,*], Gil-Seung Lee[a], Hwa-Young Kim[b], Jung-Hwan Ahn[b]

[a]*Department of Mechanical & Intelligent Systems Engineering, Pusan National University, Korea*
[b]*Department of Mechanical Engineering, Pusan National University, Korea*

(Manuscript Received August 23, 2006; Revised December 29, 2006; Accepted January 2, 2007)

Abstract

In this paper a new modeling method for an eddy current sensor is presented using geometric and electromagnetic data of a sensor and a measuring target. It can predict not only sensor output but also medium behavior related to sensor output. The geometric data of a sensor coil and the eddy current generated on a measuring target are simplified to an array of circular loops. And to perform computations of the network circuit between sensor coil loops and eddy current loops using the geometric and electromagnetic data in order to consider all possible interactions, the equivalent network circuit of eddy current sensor's behavior has been drawn. Because the sensor's initial value, medium behavior, and final value can be shown quantitatively by the proposed modeling method as the geometric and electromagnetic data varies, it can precisely predict the sensor output depending on the measuring goal and application field. Thus the model can be utilized to improve accuracy, eliminate the need for calibration before use, and produce the best design for any given purpose.

Keywords: Eddy current; Geometric; Electromagnetic; Electromotive force; Mutual inductance; Conductivity

1. Introduction

An eddy current sensor has good response time and fewer environmental limits to its use, so that it can be utilized to measure displacement or vibration of metal objects and to detect defects in metal objects without causing damage. However, the output of the eddy current sensor is nonlinear depending on the geometric shape of the sensor coil, the base metal, and the properties of the matter (1981). Thus, its accuracy is limited and must be calibrated before use. There are problems especially when continuously measuring the displacement of various metal objects. The existing modeling method is a supposition method in that the sensor coil is assumed to be an ideal solenoid (P. L. Dowell, 1966). Another modeling method is a finite element method (FEM) using Maxwell's equation (Y. Shi, D. C. Jiles, 1998; S. J. Norton, J. R., 1993). However, both methods have problems: their reliability is low due to an insufficient amount of geometric data and an unknown medium behavior related to sensor output. Consequently, experimental or experiential factors have been more valued than theory when designing an eddy current sensor (S. D. Kim and J. M. Shim, 1997; S. D. Kim, 1999; D. Vyroubal et al., 1993).

In this study, we developed a new modeling method using the geometric and electromagnetic data of a sensor coil and a measuring target (base metal) to improve the accuracy of the eddy current sensor and to eliminate the need for calibration before it is used. The resulting model was simulated using a computer and verified with an experiment.

*Corresponding author. Tel.: +82 51 510 3087; Fax.: +82 51 514 0685
E-mail address: idtaeok@naver.com

2. Modeling

2.1. Simplification of data

The same electric current flows in all parts of an eddy current sensor coil. Therefore, we can think of enough "one-turn coils" amassed concentrically on a bobbin with enough serial connections to equal the total number of sensor coil turns (N_c). One turn coil loop ($Loop_{i,j}$) is the minimum unit of coils necessary for self inductance to occur while not allowing mutual inductance to occur. The thickness of the coil loop (T_c) is equal to the thickness of the only copper substance except coating material in a sensor coil. The eddy current generated on a measuring target flows only in a tangential direction. Therefore, we can think of numerous circular loops ($Loop_k$) with different radii being laid concentrically on the same plane without being electrically connected. The loop current is determined by the impedance and the voltage induced from the sensor coil, and each eddy loop current independently flows through the circular loops. The thickness of the eddy current loop (T_e) is equal to the eddy current's effective depth of penetration. Figure 1 shows the simplified sensor coil and the eddy current's geometric data in an array of circular loops.

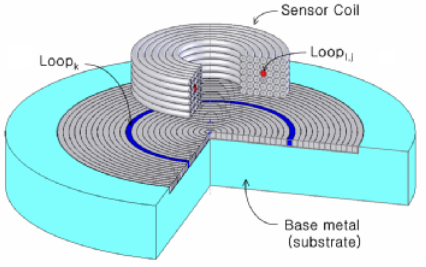

Fig. 1. Simplified sensor coil and eddy current's geometric data.

Matrices composed of the geometric and electromagnetic data are used in the model. Figure 2 shows that each row and column in the matrices is determined by each element's geometric position.

2.2. Equivalent network circuit

In this paper, we analogize the behavior between an eddy current sensor and an eddy current generated on a base metal (measuring target) to a network circuit using geometric and electromagnetic data. The computations for the network circuit were performed taking all of the possible interactions into consideration. To put it concretely, the eddy current sensor coil is role of input and output parts in the network circuit, and the eddy current generated on the base metal is role of middle part between the input and output parts. The number of independent circuits in each part is determined by the number of sensor coils and eddy current loops. The number of eddy current loops is determined by the radius of the base metal and the eddy current's effective penetration depth. The number of sensor coil loops, N_c = i×j, and the number of eddy current loops, N_e = k, are obtained from Fig. 2. Therefore, the number of independent circuits in input part is N_c, the number of independent circuits in middle part is N_e, and the number of independent circuits in output part is N_c. Weighting, which is the degree of I/O connection between independent circuits is determined by mutual inductance (M) induced from the geometric data between the loops. Function in each independent circuit is the characteristic equation of an AC equivalent circuit. The equation is a function of an impedance (L: self inductance and R: real resistance) determined by the electromagnetic and geometric data of each loop, an exciting current determined by the sensor amplifier in the input part, and an electromotive force (EMF) generated by other

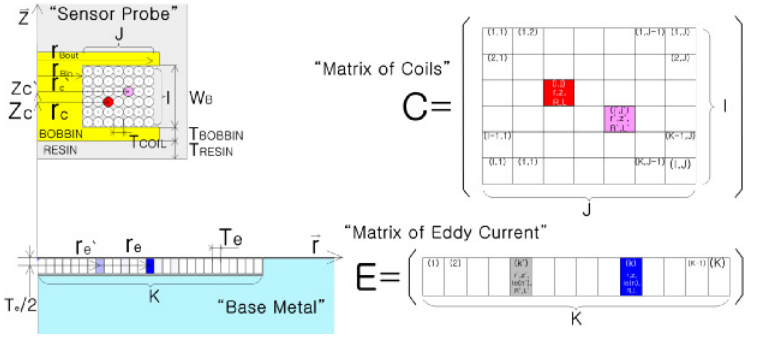

Fig. 2. Conversion geometric and electromagnetic data to ma-trix.

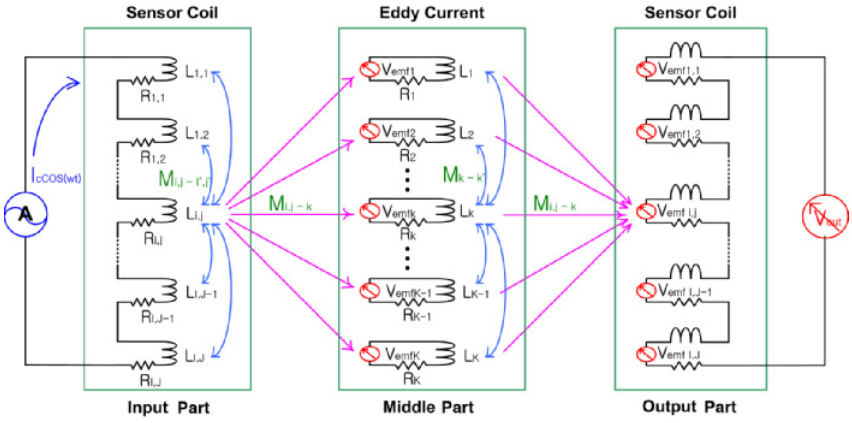

Fig. 3. Equivalent network circuit.

independent circuits in the middle and output part.

2.3. Finding factors

2.3.1. Mutual inductance (M)

Mutual inductance between two conducting wires is the degree that one's magnetic field influences the second. The magnetic field is generated by the current in the first conducting wire (P. A. Tipler, 2003; W. H. Hayt, 1981). All sensor coil loops and eddy current loops are concentric, parallel, and circular path conducting wires. The equation for the intensity of a magnetic field at any point in a circular path current is obtained by applying "Biot-Savart's law" to the geometric data as follows:

$$Id\vec{l} = -Ir_1\sin\theta\cdot d\theta\cdot\hat{i} + Ir_1\cos\theta\cdot d\theta\cdot\hat{j}$$

$$d\vec{B}_{(x)} = \frac{\mu_0 Id\vec{l}\times(\vec{d}-\vec{d}')}{4\pi\left|\vec{d}-\vec{d}'\right|^2} = \frac{\mu_0 I\left\{r_1 z\cos\theta\cdot\hat{i} + (r_1^2 - r_1 x\cos\theta)\hat{k}\right\}d\theta}{4\pi\left\{(x-r_1\cos\theta)^2 + r_1^2\sin^2\theta + z^2\right\}^{3/2}} \quad (1)$$

$$\vec{B}_{k(x)} = \int_0^{2\pi} d\vec{B}_{k(x)} = \frac{\mu_0 I}{4\pi}\int_0^{2\pi}\frac{(r_1^2 - r_1 x\cos\theta)\hat{k}\cdot d\theta}{\left\{(x-r_1\cos\theta)^2 + r_1^2\sin^2\theta + z^2\right\}^{3/2}}$$

where μ_0 is the permeability of free space, r_1, z, x, and θ are given in Fig. 4, and $\hat{i}$ is the unit vector in the x-axis direction and $\hat{j}$ is the unit vector in the y-axis direction.

The sum of all magnetic fluxes can be obtained by multiplying the intensity of the magnetic field by an infinitesimal area at any point in a plane constituted by a second conducting wire. Dividing the sum by the current amplitude of the first conducting wire, the general equation of mutual inductance can be obtained as follows:

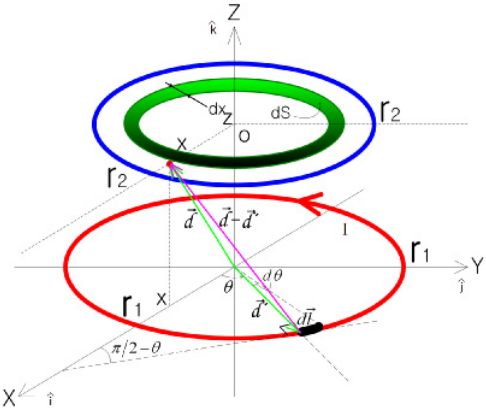

Fig. 4. Total magnetic flux in circular plane by circular path current.

$$M = \Phi / I = \frac{1}{I}\int \vec{B}_{k(x)}\, dS = \frac{1}{I}\int_0^{r_2}\vec{B}_{k(x)}\cdot 2\pi x\cdot dx$$

$$= \frac{\mu_0}{2}\int_0^{r_2} x\cdot\int_0^{2\pi}\frac{(r_1^2 - r_1 x\cos\theta)\hat{k}}{\left\{(x-r_1\cos\theta)^2 + r_1^2\sin^2\theta + z^2\right\}^{3/2}}d\theta dx \quad (2)$$

In this equation, it is important that mutual inductance is only dependent on the geometric data and is independent of the electromagnetic data. Accordingly, the equations of mutual inductance between coil loop and coil loop $M_{i,j\text{-}i',j'}$, mutual inductance between eddy current loop and eddy current loop, $M_{k\text{-}k'}$, and mutual inductance between coil loop and eddy current loop, $M_{i,j\text{-}k}$ are all the same.

2.3.2. Self inductance (L)

Self inductance is the degree that the magnetic field generated by the conducting wire influences itself (P.

A. Tipler, 2003; W. H. Hayt, 1981). The intensity of the outer conducting wire's magnetic field can be obtained using Eq. (1). However, "Biot-Savart's law" cannot be used to obtain the intensity of the inner wire's magnetic field because the current amplitude of the inner closed magnetic flux in the conducting wire varies over all points of inner section of wire. So, "Ampere's law" was utilized to derive the intensity of the magnetic field of the inner conducting wire.

2.3.2.1. Self inductance of the coil loop ($L_{i,j}$)

Figure 5 shows that the cross section of the coil loop is circular-shaped and that the field where the intensity of the magnetic field varies is classified as outer and inner. The intensity of the magnetic field of the inner coil loop decreases linearly as it goes to the center of the coil. The total magnetic fluxes in each field are

$$\Phi_1 = \frac{\mu_0 I}{2}\int_0^{r_{i,j-Tc/2}} r \cdot \int_0^{2\pi} \frac{(r_{i,j}^{\,2} - r_{i,j} r\cos\theta)}{\left\{(r - r_{i,j}\cos\theta)^2 + r_{i,j}^{\,2}\sin^2\theta\right\}^{3/2}} \cdot d\theta dr \quad (3)$$

and $\Phi_2 = \mu_0 I \cdot \int_{r_{i,j-Tc/2}}^{r_{i,j}} \left[\frac{r_{i,j} - r}{(Tc/2)^2} + \frac{1}{(r_{i,j}+r)^2}\right] \cdot r \cdot dr$,

respectively, (4)

and the self inductance of the coil loop is

$$L_{i,j} = (\Phi_1 + \Phi_2)/Ic \quad . \quad (5)$$

2.3.2.2. Self inductance of the eddy current loop (L_k)

For the ease of modeling, the eddy current generated on the base metal was simplified in order to combine it with square-shaped loops. The side of square, T_e, is determined by the length of the eddy current's effective depth of penetration (Z. Molttl, 1990), and each loop's radius, r_e, is different. Figure 6 shows that cross section of the eddy current loop is square-shaped and that the field where the intensity of the magnetic field varies is classified as outer, overlapping, and inner. The variation of the intensity of the magnetic field in the overlapping section is nonlinear. The total magnetic fluxes of the outer and the inner fields are the same as in Eqs. 3 and 4. The total magnetic flux in the overlapping field and self inductance of the eddy current loop are

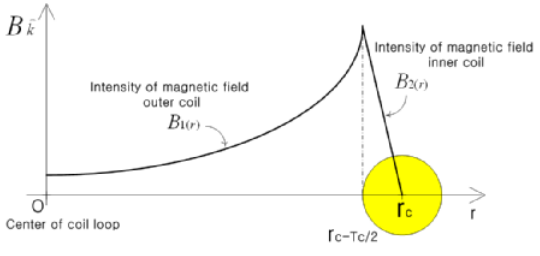

Fig. 5. Variation of intensity of the magnetic field by coil loop.

$$\Phi_3 = \mu_0 I \int_{r_{k-Te/\sqrt{2}}}^{r_{k-Te/2}} \left[\frac{2\left\{(r_k - r)Te\sin(\varphi) + 2(r_k - r)^2(\pi/4 - \varphi)\right\}}{rTe^2} \cdot \right.$$

$$\left. \cdot + \frac{1}{(r_k + r)^2}\right] r\,dr$$

and $L_k = (\Phi_1 + \Phi_{2+}\Phi_3)/I$, (7)

where $\varphi = \cos^{-1}\left\{Te/2(r_k - r)\right\}$.

2.3.3. Real resistance (R_{AC})

Resistance to an AC current is greater than to a DC current because of the 'skin effect' in the conducting wire itself and the 'proximity effect' from the other conducting wire [12]. The increment of resistance in an AC current is not only related to the electromagnetic data (frequency, conductivity) but also to the geometric data (positions of conducting wires) (H. A Wheeler., 1942). The prospect of an incremental rate of resistance, R_{ratio}, has been heavily investigated in the electric power field but so far a general equation has not been presented (Y. J. Wang, 1999; Y. Iwashita, 2004). Therefore, it is difficult to use a theory to obtain the R_{ratio} of conducting wires that have been complexly amassed as in the eddy current sensor, so it has been obtained experimentally. In this paper, we assume that Rc_{ratio} of the coil loop is 1 (one) because the resistance increment is insignificant for lower frequencies than 500㎑. Also, we assume that Re_{ratio} of the eddy current loop is 1 (one) because the real boundary surface between adjacent eddy current loops is absent. Therefore, the real resistance of the coil loop at the *i-th* low and the *j-th* column, $R_{i,j}$, and the real resistance of the eddy current loop at the *k-th* column, R_k, are

$$R_{i,j} = (1 + \alpha c \cdot \Delta t) \cdot Rc_{ratio} \cdot \frac{2 \cdot r_{i,j}}{\sigma c \cdot (Tc/2)^2} \quad (8)$$

and $R_k = (1 + \alpha e \cdot \Delta t) \cdot \frac{2\pi \cdot r_k}{\sigma e \cdot Te^2}$, respectively, (9)

where α is the temperature coefficient of resistance, Δt is the deviation in temperature from *20* ℃, and σ is the electrical conductivity. In these equations, $r_{i,j}$, r_k,

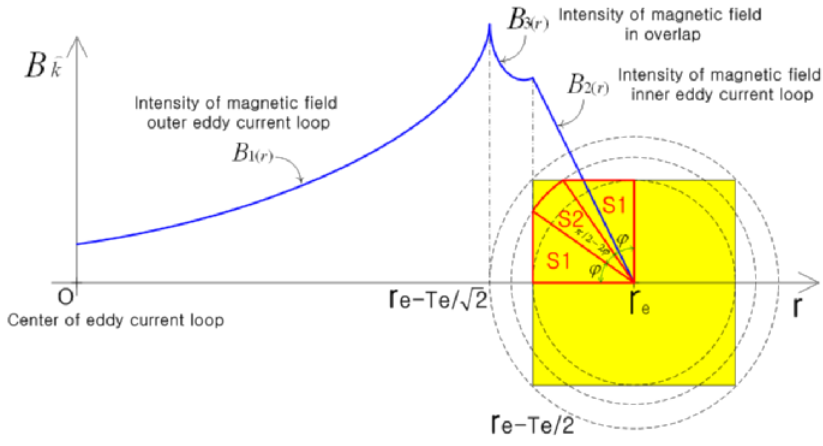

Fig. 6. Variation of intensity of the magnetic field by eddy current loop.

T_c, and T_e are given in Fig. 2, and the subscripts c and e denote the sensor coil loop and eddy current loop, respectively.

3. Each part computation in network circuit

3.1. Initial value of sensor

When the eddy current sensor probe is in the air the distance between the sensor and the base metal is infinite, and the initial impedance of the sensor is

$$R_0 = \sum_{Nc} R_{i,j} \tag{10}$$

$$L_0 = \sum_{Nc}\left(L_{i,j} + \sum_{Nc-1} M_{i,j-i',j'}\right) \tag{11}$$

$$Z_0 = \sum_{Nc} R_{i,j} + jw\left(\sum_{Nc}(L_{i,j} + \sum_{Nc-1} M_{i,j-i',j'})\right) \cdot \tag{12}$$

where $w = 2\pi f$.

When the exciting current with a zero phase in the coil is

$$I_{c(j\omega)} = I_c \cdot e^{i0} \tag{13}$$

the initial voltage of the sensor is

$$V_{0(j\omega)} = Z_{0(j\omega)} \cdot I_{c(j\omega)}$$

$$= \left[\sum_{Nc} R_{i,j} + jw\left(\sum_{Nc}(L_{i,j} + \sum_{Nc-1} M_{i,j-i',j'})\right)\right] \cdot I_c \tag{14}$$

3.2. Medium behavior of sensor

The medium behavior between the eddy current sensor and the measuring target (base metal) related to the sensor's output is given below. The electromotive force (EMF) in each eddy current loop by all of the sensor coil loops is

$$V_{emf\,k(j\omega)} = -j \cdot w \cdot I_c \cdot \sum_{Nc} M_{i,j-k} \ , \tag{15}$$

and the impedance of each eddy current loop is

$$Z_{k(j\omega)} = R_k + jw(L_k + \sum_{Ne-1} M_{k-k'}) \tag{16}$$

From Eqs. (15) and (16), the current in each eddy current loop is obtained as follows

$$I_{k(j\omega)} = V_{emf\,k(j\omega)} / Z_{k(j\omega)} = \left\{-j \cdot w \cdot I_c \cdot \sum_{Nc} M_{i,j-k}\right\} \left\{R_k + jw(L_k + \sum_{Ne-1} M_{k-k'})\right\} \tag{17}$$

Consequently, the electromotive force in each sensor coil loop by all of the eddy current loops is

$$V_{emf\,i,j(j\omega)} = \sum_{Ne} v_{emf(eddy \rightarrow coil)} = -j\omega \cdot \sum_{Ne} M_{i,j-k} \cdot I_{k(j\omega)} \tag{18}$$

3.3. Final output of sensor

When the eddy current sensor probe is near the base metal, the output voltage of the sensor is

$$V_{out(j\omega)} = Z_{0(j\omega)} \cdot I_{c(j\omega)} + \sum_{Nc}\sum_{Ne} v_{emf(eddy \rightarrow coil)}$$
$$= \left[\sum_{Nc} R_{i,j} + jw\left(\sum_{Nc} (L_{i,j} + \sum_{Nc-1} M_{i,j-i',j'}) \right) \right]$$
$$\cdot I_{c(j\omega)} - j\omega \cdot \sum_{Nc}\sum_{Ne} M_{i,j-k} \cdot I_{k(j\omega)} \quad (19)$$

and the impedance of the sensor is

$$Z_{s(j\omega)} = V_{out(j\omega)} / I_{c(j\omega)}$$
$$= \left[\sum_{Nc} R_{i,j} + jw\left(\sum_{Nc} (L_{i,j} + \sum_{Nc-1} M_{i,j-i',j'}) \right) \right]$$
$$- \left(j\omega \cdot \sum_{Nc}\sum_{Ne} M_{i,j-k} \cdot I_{k(j\omega)} \right) \Big/ I_{c(j\omega)} . \quad (20)$$

Then, variations of the sensor's impedance are

$$\Delta Z_s = Z_s - Z_0 = -\left(j\omega \cdot \sum_{Nc}\sum_{Ne} M_{i,j-k} \cdot I_{k(j\omega)} \right) \Big/ I_{c(j\omega)}, \quad (21)$$

$$\Delta R_s = -\mathrm{Re}\left[\left(j\omega \cdot \sum_{Nc}\sum_{Ne} M_{i,j-k} \cdot I_{k(j\omega)} \right) \Big/ I_{c(j\omega)} \right], \quad (22)$$

and

$$\Delta L_s = -\mathrm{Im}\left[\left(j\omega \cdot \sum_{Nc}\sum_{Ne} M_{i,j-k} \cdot I_{k(j\omega)} \right) \Big/ I_{c(j\omega)} \right]. \quad (23)$$

4. Result and verifications

The geometric and electromagnetic data for the eddy current sensor and the base metal used in the model and in the verification experiment are shown in Table 1. The technical computing language, MATLAB, was used to simulate the model. The properties of the specimens (base metal, measuring target) were determined by the Korea Research Institute of Standards and Science (KRISS). A precision positioning system (resolution = 20 nm) for varying the distance between the sensor and the specimen from 0 to 2.5 mm and an LCR meter (KOKUYO, KC-605) for measuring the changes of impedance were used in the experiment. Figure 7 shows the experiment system.

4.1. Initial value of sensor

When the frequency of the exciting current was *100㎑*, the initial real resistance of the sensor coil obtained by experimental measurement, and by simulation of the model were *3.3057Ω* and *3.3094Ω*, respectively. Consequently, the error was *-0.0037Ω*, and the reliability was *99.89%*. Although we assumed

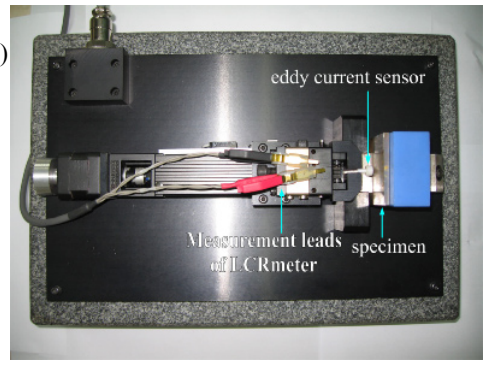

Fig. 7. Photograph of precision positioning system and specimen.

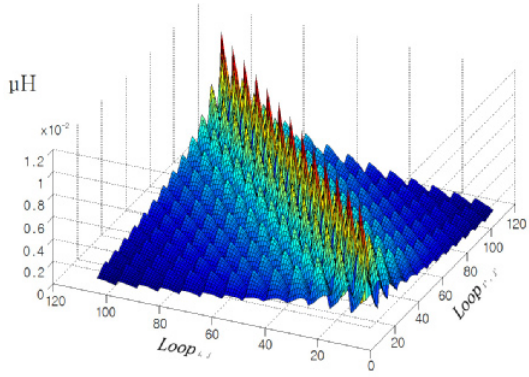

Fig. 8. Initial total inductance of coils.

that the sensor coil's rate of resistance increment (R_{Cratio}) was 1 (one), almost no error was present. Perhaps the small error was due to omitting the temperature coefficient of resistance (α_c). The error increased as the frequency increased, especially when the frequency was over *500㎑*. The total inductances, the summation of self inductance and mutual inductance between the coil loops, obtained by experimental measurement and by simulation of the model were *37.2690μH*, *37.0780μH*, respectively. Consequently, the error was *0.1910μH* and the reliability was *99.48%*. To sum up, the initial real resistance error was mainly caused by the omission of R_{Cratio} and the difference between the simplified geometric data and the real geometric data of the sensor coils, and the initial inductance error was dependent upon the simplification of the geometric data of the sensor coil (Fig. 1) and the winding error of the coils when the sensor was manufactured because inductance depends solely on the geometric data.

Table 1. Geometric and electromagnetic data used in the model and experiment.

		Geometric data				Electromagnetic data		
SENSOR	Bobbin	Width where coil were wound on (Z-direction)	W_B	1.42	(mm)			
		Minimum radius where coil occupy	r_{Bin}	1.47	(mm)	material		epoxy
		Maximum radius where coil occupy	r_{Bout}	2.23	(mm)	conductivity(σ)		0 (%IACS)
		Thickness of bobbin and resin near to base metal	T_B	0.5	(mm)	relative permeability(μr)		1
	Coil	Total number of coil loop (coil turns)	N_C	$I \times J = 104$	(Turn)			
		Number of loop in Z-direction	I	13	(Turn)	material		Cu
		Number of loop in R-direction	J	8	(Turn)	conductivity(σ)		99.9 (%IACS)
		Thickness of coil(only conductor)	T_C	0.09	(mm)	relative permeability(μr)		1
		Thickness error in Z-direction by enamel and manufacture	T_{CZ} $_{error}$	$W_B/K-T_C$ =1.923×10E-5	(mm)	Ic		0.001(A)
						Frequency		100(KHz)
		Thickness error in R-direction by enamel and manufacture	T_{CR} $_{error}$	$(RBout-RBin)/J-T_C$ =3.75×10E-6	(mm)			
SPECIMEN	Base Metal	Width	W_m	60	(mm)	material	conductivity (%IACS)	relative permeability(μr)
		Length	L_m	60	(mm)	SUS304	2.47	1
		Thickness	T_m	5	(mm)	Ti	3.72	1
	Eddy Current	Effective depth of penetration	T_e	$1/(e\times\pi\times f\times\mu_r\times\mu_0\times\sigma)^{1/2}$	(mm)	Brass	24.39	1
						AL6061	42.02	1
		Number of eddy current loop	K	$W_m/2T_e$	(Turn)	Cu	99.2	1

Figure 8 shows the model's initial total inductance of the sensor coils.

The sensor's initial voltage in the model was about *233mV* and reliability was *99.49 %*.

4.2. Medium behavior of sensor

4.2.1. Total inductance of eddy current loops

Figure 9 shows the total inductance of the eddy current loops which are composed of the self inductance (L_k) of the eddy current loop itself and the mutual inductance ($M_{k\text{-}k'}$) between the eddy current loops. The summation of the inductance of each eddy current loop increased exponentially as the radius of eddy current loop increased. However, it is important to note that the summation of the inductance decreased slightly near the edge of the specimen. This medium behavior is result of the self inductance (L_k) of eddy current itself increasing as the radius of eddy current loop increases because the generated magnetic flux is proportional to the radius of the loop. Also, this behavior is result of the summation of mutual inductance between the eddy current loops decreasing

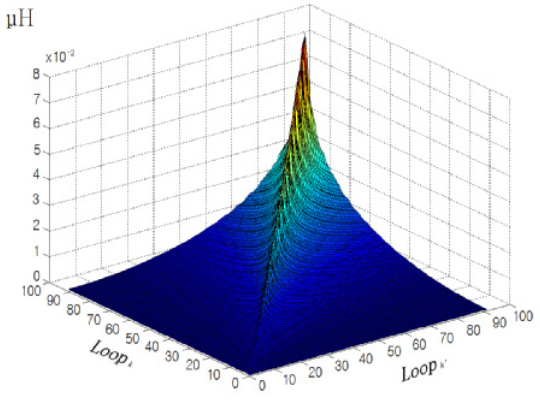

Fig. 9. Total inductance of eddy current loops.

near the edge of the specimen because the number of eddy current loops decreases relative to the inner range of the specimen, that is to say, because there are no eddy current loops on the outside of specimen. This situation influenced the amplitude distribution of the current in each eddy current loop (I_k).

4.2.2. Mutual inductance between coil loop and eddy current loop ($M_{i,j-k}$)

Mutual inductance ($M_{i,j-k}$) is directly related to the sensitivity of the eddy current sensor. Especially, the final goal will be to obtain the mutual inductance between the sensor coil and the eddy current when we want to measure the distance and the vibration of metal. Fig.10 shows the mutual inductance between the sensor coil and the eddy current loops. In Fig. 10 (a) it can be seen that the sensor coil loop closer to the eddy current loop generated on the specimen (base metal, measuring target) has greater influence on the sensor output. Also, in Fig. 10 (b) it can be seen that the eddy current loop located at a far place from center and just under a sensor coil loop has greater influence on the sensor output when the sensor is far from the measuring target. Therefore, to obtain good results when designing a new sensor, the sensor coil loops must be placed in a position where the mutual inductance ($M_{i,j-k}$) has been largely influenced by the eddy current loop. And also, we can design the most suitable shape, radius, and length for a sensor with good sensitivity by taking into consideration that the mutual inductance ($M_{i,j-k}$) is dependent on the initial offset from the sensor to the specimen and measurement range.

4.2.3. Electromotive force in each eddy current loop

Figure 11 was obtained from Eq. (15), and shows the amplitude distribution of electromotive force in the eddy current loop. From Fig. 11, it is clear that the mutual inductance ($M_{i,j-k}$) between the sensor coil loop ($Loop_{i,j}$) and the eddy current loop ($Loop_k$) varies according to the distance between the sensor coil and the specimen (base metal), as a result of it, the electromotive force in each eddy current loops by the sensor varies.

4.2.4. Amplitude of current in each eddy current loop (I_k)

The larger the amplitude of current in each eddy current loop is, the larger the output of the sensor is. The prominent factors influencing the amplitude of the eddy current are impedance (Z_k), self inductance

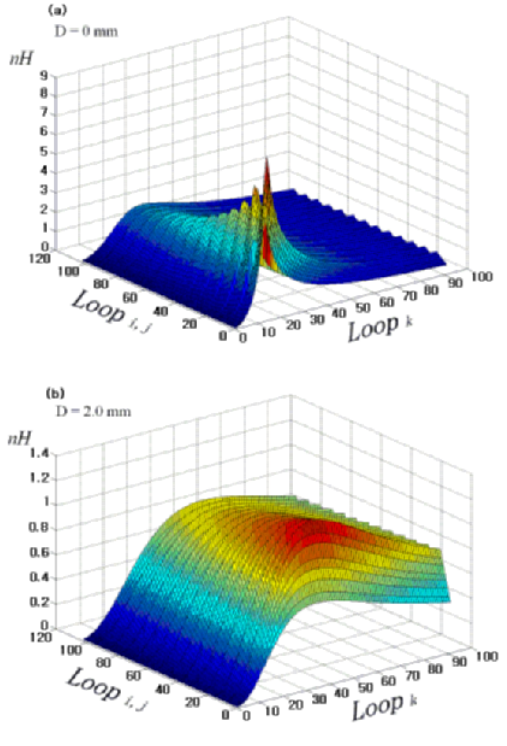

Fig. 10. Mutual inductance between the sensor coil loop and the eddy current loop at (a) gap(D) = *0㎜* and (b) gap(D) = *2.0㎜*.

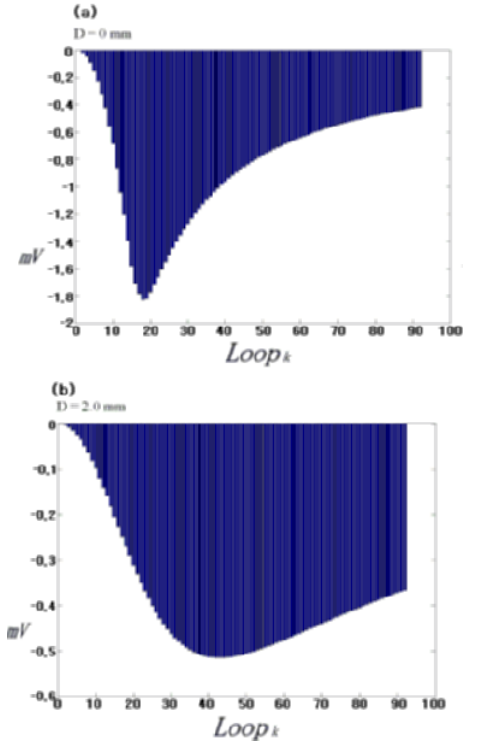

Fig. 11. Electromotive force in each eddy current loops at (a) gap(D) = *0㎜* and (b) gap(D) = *2.0㎜*.

(L_k), and mutual inductance ($M_{k\text{-}k'}$) in each eddy current loop. Figure 12 was obtained from Eq. (17), and shows the amplitude distribution of current in each eddy current loop. As the radius of the eddy current loop increased, the amplitude of the eddy current increased in the region just under the sensor coil and decreased outside of the sensor coil. However, the amplitude of the eddy current increased slightly near the edge of the specimen. This phenomenon is due to the summation of the mutual inductance between the eddy current loops decreasing near the edge of the specimen. This phenomenon does not occur when the region of the base metal effected by the sensor coil is sufficiently large, i.e. the radius of the base metal is sufficiently large than the radius of the sensor coil. This phenomenon can be used to measure the radius of the base metal.

4.2.5. Electromotive force in each coil loop ($V_{emf\,i,j}$)

The electromotive force in each sensor coil loop, which is determined by the total current in each eddy current loop and by the mutual inductance between the sensor coil loop and the eddy current loop, directly influenced the output of eddy current sensor. Figure 14 was obtained from Eq. (18), and shows the electromotive force in each coil loops.

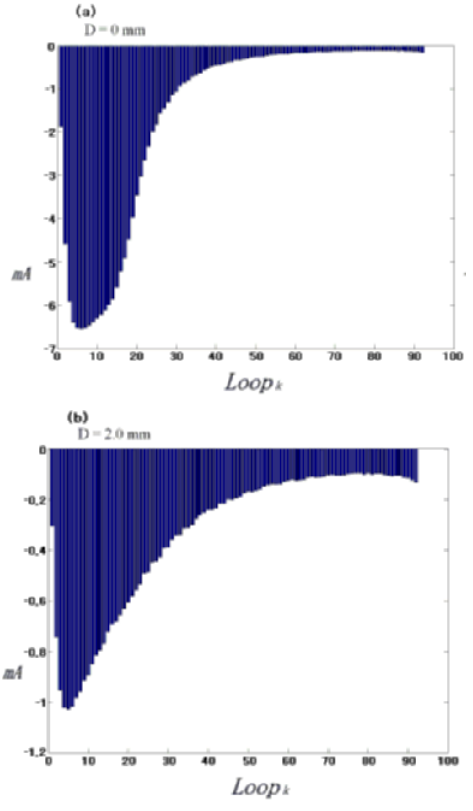

Fig. 12. Amplitude of current in each eddy current loop at (a) gap(D) = *0㎜* and (b) gap(D) = *2.0㎜*.

4.3. Final output of the sensor

Figure 14, obtained from Eq. (20), shows the impe-

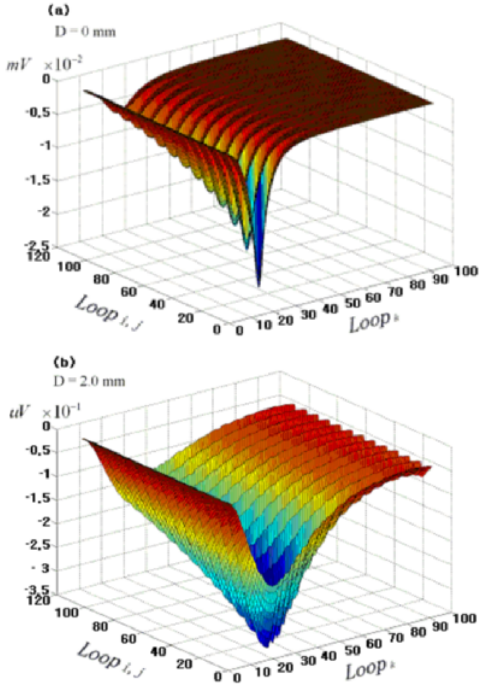

Fig. 13. Electromotive force in each coil loop at (a) gap(D) = *0㎜* and (b) gap(D) = *2.0㎜*.

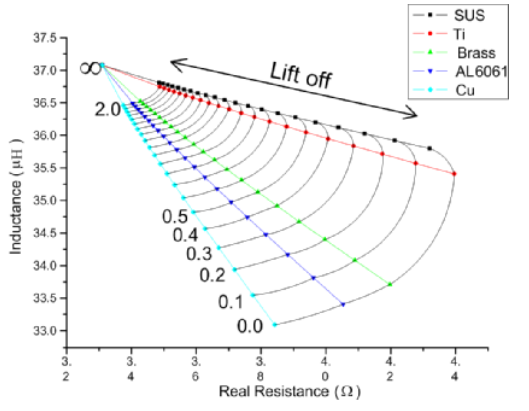

Fig. 14. Impedance plane made varying the distance between the sensor and the specimen (base metal, measuring target).

dance variations by the distance (lift off) between the sensor and the base metal and by the properties of the base metal. From Fig. 14, it can be seen that the slopes (ΔL/ΔR) are constant when the range of measurements is between zero and infinity. The slope (ΔL/ΔR) error is bigger for SUS304 than for the others. This may be due to the specimen (base metal) being thinner than the effective penetration depth of the eddy current. By sensing these slopes which could be obtained as comparison initial sensor impedance with sensor impedance when probe is near to the base metal, the physical properties of the base metal could be identified, and this result can be utilized to eliminate the need for calibrating the sensor to different material target before use through multiplying sensor output by correct weighting which is drawn from modeling result (Fig.17).

Figure15 shows the variations in the sensor's inductance obtained from Eq. (23) and the modeling errors by experimental result. The most sensitive specimen is copper because it is a better conductor than the others. Therefore, in case of a base metal being copper, it had the largest modeling error and the inductances of sensor obtained by experimental measurement and by simulation of the model were *32.4613 μH* and *33.0930 μH*, respectively. Consequently, the error was *-0.6317 μH*, and the reliability was *98.05%*. When the measurement distance is zero, the error does not match the other patterns. This was because the positioning system used in the experiment could not move the sensor so that the distance between the sensor and the base metal (specimen) was zero.

Figure 16 shows the variations of the sensor's resistance obtained from Eq. (22) and the modeling errors by experimental result. In the experimental result, the increment of resistance becomes slightly larger as the sensor nears the base metal. This may be due to the proximity effect between the current in sensor coil and the eddy current on the base metal. Therefore, in case of a base metal being copper, the real resistance of sensor had the largest resistance error and the real resistances of sensor obtained by experimental measurement and by simulation of the model were *3.8312 Ω* and *3.8417 Ω*, respectively. Consequently, the error was *-0.0105 Ω*, and the reliability was *99.73%*. When the measurement distance is zero, the error did not match the patterns of the others for the same reasons as before.

Figure 17 shows the variations of the sensor's voltage output obtained from Eq. (19) and the modeling errors by experimental result. In experiment, copper that had the highest conductivity among base metals had the largest voltage error in the model. In case of a base metal being copper, the voltage outputs obtained

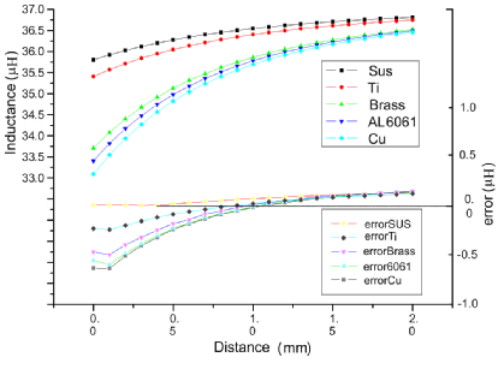

Fig. 15. Variations and errors of the inductance of sensor.

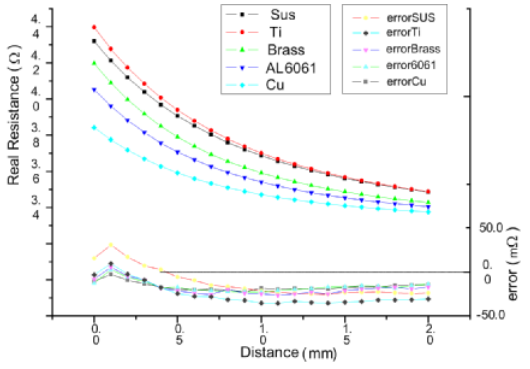

Fig. 16. Variations and errors of sensor resistance

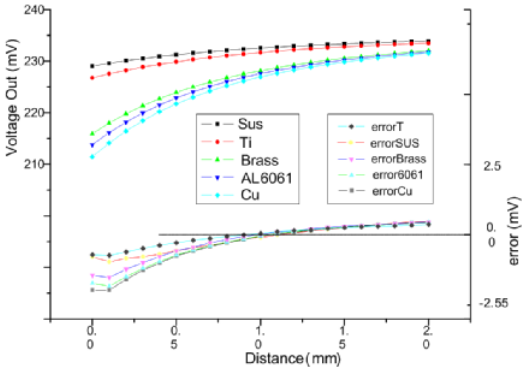

Fig. 17. Variations and errors of sensor's voltage output.

by experimental measurement and by simulation of the model were *211.4500 mV* and *213.4100 mV*, respectively. Consequently, the error was *-1. 9600 mV* and the reliability was *99.07%*.

5. Conclusions

In this paper, a new modeling method was presented using the geometric and electromagnetic data of a sensor coil and a base metal (measuring target). We simplified the sensor coil and the eddy current's geometric data into an array of circular loops. The physical behavior between the eddy current sensor and the eddy current generated on a measuring target was analyzed by performing computations of the equivalent network circuit between sensor coil loops and eddy current loops using the geometric and electromagnetic data so that all possible interactions could be considered. The new model was simulated with a computer (MATLAB®) and verified with an experiment. The new modeling method presented in this paper can predict the initial and final sensor's output. In addition, the model can quantitatively present the medium behavior related to sensor's output. If the increment of resistance by an AC current, R_{ratio}, for any frequency is known either from experimental data or from a manufacturer, it can be used in the model to obtain more accurate solutions. This modeling method can be utilized to improve accuracy, eliminate the need for calibration before use, and produce the best design for any given purpose.

References

"Eddy Current Characterization of Materials and Structures," ASME Special Technical Publication, American Society for Testing and Materials, 1981.

Dowell, P. L., 1966, "Effects of Eddy Currents in Trans former Windings," *Proc. IEE*, Vol. 113 No. 8.

Cheng, C. C., Dodd, C. V., Deeds, W. E., 1971, "General Analysis of Probe Coils Near Stratified Conductors," *Int. J. Nondestruct. Test.,* Vol. 3, pp. 109~130.

Shi, Y., Jiles, D. C., 1998, "Finite Element Analysis of the Influence of a Fatigue Crack on Magnetic Properties of Steel," *J. Appl. Phys.*, Vol. 83 No. 11, pp. 6353~ 6355.

Norton, S. J., Bowler, J. R., 1993, "Theory of Eddy Current Inversion," *J. Appl. Phys.*, Vol. 73, pp. 501~512.

Kim, S. D., Shim, J. M., 1997, "Impedance Analysis and Experimental Study of a Solenoid Eddy Current Sensor to Detect the Cross Section Area of Non Ferromagnetic Stranded Conductors," *J. of Korea Sensor Society*, Vol. 6 No. 2, pp.87~94.

Kim, S. D., 1999, "An Experimental Study on a Solenoid Eddy Current Sensor to Inspect Deterioration in Overhead Distribution Lines," *J. of Korea Institute of Illuminating and Electrical Installation Eng.*, Vol. 13 No. 1, pp. 77~85.

Vyroubal, D., et al., 1993, "Experimental Optimization of the Probe for Eddy Current Displacement Transducer," *IEEE Trans. Instrum. Meas.*, Vol. 42, pp. 99~1000.

Tipler, P. A., Mosca, G., 2003, "Physics 5/E:for Scientists and Engineers," *Freeman*.

Hayt, W. H., 1981 "Engineering Electromagnetics," *Mc-Graw-Hill*.

Molttl, Z., 1990, "The Quantitative Relation Between True and Standard Depth of Penetration of Air-Cored Probe Coils in Eddy Current Testing," NDT International, Vol. 23 No. 1, pp. 11~18.

"Proxy. A Proximity and Skin Effect Analysis Program," *KO Systems*.

Wheeler., H. A., 1942, "Formulas for the Skin-Effect," *Pro-eedngs of the Institute of Radio Engineers*, Vol. 30, pp. 12~24.

Wang, Y. J., 1999, "Analysis of the Skin Effect for Cal-ulating Frequency-Dependent Impedance of the TRTS Power Rail," Proc. Natl. Sci. Counc. ROC, Vol. 23 No. 3, pp. 419~428.

Iwashita, Y., 2004. "Reduction of RF Power Loss Caused by Skin Effect," *Proceedings of LINAC 2004, THP43*, pp. 700~702.